Remote Sensing of Environment 284 (2023) 113347

Contents lists available at ScienceDirect

Remote Sensing of Environment

journal homepage: www.elsevier.com/locate/rse

Interannual changes of coastal aquaculture ponds in China at 10-m spatial resolution during 2016–2021

Ming Wang [a,b], Dehua Mao [a,*], Xiangming Xiao [c], Kaishan Song [a], Mingming Jia [a], Chunying Ren [a], Zongming Wang [a,d]

[a] Key Laboratory of Wetland Ecology and Environment, Northeast Institute of Geography and Agroecology, Chinese Academy of Sciences, Changchun 130102, China
[b] University of Chinese Academy of Sciences, Beijing 100049, China
[c] Department of Microbiology and Plant Biology, Center for Earth Observation and Modeling, University of Oklahoma, Norman, OK 73019, USA
[d] National Earth System Science Data Center, Beijing 100101, China

ARTICLE INFO

Edited by Menghua Wang

Keywords:
Coastal aquaculture ponds
Sentinel-2 imagery
Coastal wetlands
Google Earth Engine
China

ABSTRACT

The rapid growth of coastal aquaculture has strongly supported global food security and economic development of coastal areas in the past few decades but has also caused remarkable impacts on coastal ecosystems. Accurate delineation of coastal aquaculture extent and changes is thus significant for improving coastal zone management toward sustainability. Here, by means of Sentinel-2 images, we propose an effective and rapid approach that combines simple non-iterative clustering (SNIC) with hierarchical decision trees (HDT), so-called SNIC-HDT, to generate fine-resolution coastal aquaculture pond data at the national scale of China. The SNIC-HDT fully considers the spatial heterogeneity of coastal aquaculture ponds and performs accurate segmentation by determining the optimal segmentation scale for coastal aquaculture ponds with different sizes and shapes. In addition, the SNIC-HDT incorporates temporal features into the establishment of HDT and thus effectively distinguishes coastal aquaculture ponds from other water bodies. In support of the Google Earth Engine platform, we employed 85,501 scenes of Sentinel-2 images and generated the first annual 10-m spatial resolution national coastal aquaculture pond dataset of China between 2016 and 2021 (China_CAP), with an overall classification accuracy of more than 90%. This dataset reveals that total area of China's coastal aquaculture ponds experienced a substantial loss of 13.21% from 9769 km^2 in 2016 to 8629 km^2 in 2021. The most remarkable areal reduction occurred in Zhejiang Province, with a decrease rate of 38.24%, followed by Guangdong (27.93%), and these reductions were mostly related to the policy of retuning aquaculture ponds to natural wetlands. Coastal aquaculture ponds in Fujian and Tianjin provinces experienced slight areal gains (7.24% and 2.13%). The results generated in this study could provide a basis for the conservation of habitats of migratory water birds on the East Asia-Australia Flyway and are of great scientific and practical importance to support the evaluation of Sustainable Development Goals.

1. Introduction

Coastal aquaculture ponds which are used for aquaculture and include dams in coastal areas, have expanded rapidly worldwide and played a critical role in the global food security and socioeconomic development of coastal zones (Ottinger et al., 2016; Suweis et al., 2015; Tacon, 2020). However, the expansion of coastal aquaculture ponds has also caused serious environmental issues, such as natural habitat loss, water eutrophication, and ecosystem degradation (Ahmed et al., 2019; Gephart et al., 2021). According to the United Nations Food and Agriculture Organization (FAO), China is the world's largest aquaculture food producer, contributing approximately 61.5% of global production (FAO, 2020). Coastal aquaculture ponds have rapidly expanded in China due to extensive land conversion in recent decades, with a net increase of approximately 10,463 km^2 and a rate of 327 km^2 per year from 1984 to 2016 (Ren et al., 2019). Such rapid expansion poses serious threats to China's coastal ecosystems and biodiversity, causing the loss and degradation of tidal flats and mangroves that are important to migratory birds (Jia et al., 2021; Mao et al., 2022; Wang et al., 2020). Although previous studies have provided national-scale datasets of coastal

* Corresponding author.
E-mail address: maodehua@neigae.ac.cn (D. Mao).

https://doi.org/10.1016/j.rse.2022.113347
Received 18 August 2022; Received in revised form 1 November 2022; Accepted 3 November 2022
Available online 12 November 2022

aquaculture ponds in China (Duan et al., 2021; Ren et al., 2019), those data are outdated and limited to coastal ecosystem planning and management particularly due to their moderate spatial resolution (30-m) and temporal resolution (5 or 10 years). Therefore, an accurate and up-to-date coastal aquaculture pond dataset with a finer resolution is urgently needed for sustainable management and conservation of coastal ecosystems, especially since the implementation of the Sustainable Development Goals (SDGs) in 2015.

Various satellite data sources have been employed to identify coastal aquaculture ponds around the world. High spatial resolution optical images, such as Rapid-Eye, SPOT-5 and WorldView-2, have shown great potential in delineating coastal aquaculture ponds due to the advantage in identifying the dams (Fu et al., 2019; Sridhar et al., 2008; Virdis, 2014), but they are frequently expensive and limited in spatial and temporal coverages, making them insufficient for large-scale mapping. While Landsat images with moderate spatial resolution (30-m) have been extensively used to identify coastal aquaculture ponds due to their broad and long-term coverage (Duan et al., 2021; Ren et al., 2019), however, it is frequently difficult to correctly detect dams around ponds and thus resulting in low accuracy and large uncertainty. Sentinel-1 imagery has been increasingly employed in mapping coastal aquaculture ponds in recent years due to its capability of all-weather and day-night acquisition, such as in coastal Vietnam and India (Prasad et al., 2019; Sun et al., 2020). Although synthetic aperture radar (SAR) images from Sentinel are largely unaffected by clouds compared to optical images, they have more speckle and border noises that are difficult to suppress effectively, significantly decreasing the signal-to-noise ratio and radiometric resolution (Ali et al., 2018). Additionally, due to the unique SAR imaging mechanism, edge features, such as the dams surrounding the coastal aquaculture pond, are typically over-amplified in the image, resulting in substantial uncertainty in mapping aquaculture pond using Sentinel-1 SAR data. In contrast, Sentinel-2 imagery is ideal satellite resource for mapping large-scale coastal aquaculture ponds due to their abundant spectral information, fine spatial resolution (10-m) and temporal resolution (2–5 days), which are beneficial to the detection of dams and the characterization of seasonal changes in coastal aquaculture ponds.

Coastal aquaculture ponds have similar spectral characteristics to other surface waters in coastal areas and exhibit spatial heterogeneity in water color, shape, and size, which causes difficulty in mapping them at a broad scale by satellite images. Although many supervised machine learning methods, such as random forest and deep learning, have been achieved in mapping coastal aquaculture ponds in different countries or regions (Diniz et al., 2021; Xia et al., 2020), these methods usually require a combination of complex pre- and post-processing to obtain a reliable product, which may not be applicable to large-scale studies. Object-oriented decision tree classification identifies coastal aquaculture ponds by constructing decision trees comprising various landscape features by generating image objects using empirical segmentation thresholds, and has been widely used for mapping coastal aquaculture ponds (Fu et al., 2019; Loberternos et al., 2016; Ottinger et al., 2016). Disregarding variances in size and shape of coastal aquaculture ponds among regions, using a single segmentation threshold for a broad scale may have a negative effect on the accuracy of subsequent classification (Johnson and Xie, 2011). Additionally, since the sizes, shapes, and spectra of coastal aquaculture ponds and other surface water bodies such as salt pan are highly similar, employing simple object features extracted from a single image without considering their different characteristics resulting from seasonal changes is insufficient for separating them and may result in misclassification (Zhang et al., 2022). Given these issues, a practical method for mapping large-scale coastal aquaculture ponds that fully considers spatial heterogeneity and temporal changes in coastal aquaculture ponds is needed, especially for the largest developing country, China.

Using the time series Sentinel-2 remotely sensed data on the Google Earth Engine platform (GEE), we developed an object-oriented method combining hierarchical decision trees (HDT). The first annual maps of coastal aquaculture ponds in China with a 10-m spatial resolution from 2016 to 2021 were generated. The up-to-date spatial distribution and temporal changes of coastal aquaculture ponds were also examined at the provincial and national scales. The generated results are expected to support sustainable planning and management of China's coastal zones and facilitate the evaluation of related targets of SDGs.

2. Materials and methods

2.1. Study area

China's coastal zone spans more than 20 degrees of latitude between the estuary of the Yalu River in the north and the estuary of the Beilun River in the south (18.2°N to 40.5°N) (Fig. 1). The main wetland landscapes of coastal zones are tidal flat, mangrove forest, salt marsh, coastal aquaculture pond and shallow marine water (Mao et al., 2020). Coastal aquaculture ponds are extensively distributed across the coastal zone, usually comprising various shapes and sizes due to significant variations in geographic and climatic conditions (Fig. 1A-D). The study area is defined as the zone between a 20-km buffer line landward and a 10-km buffer line seaward from the coastline, which can cover all coastal aquaculture ponds, based on a series of field survey and visual interpretation of the latest Google Earth images.

2.2. Data and preprocessing

2.2.1. Sentinel-2 images and preprocessing

All available Level-1C Sentinel-2 data covering the entire study area between 2015 and 2021 (85,501 images) were collected leveraging the GEE platform. For each image, the low-quality observations caused by cloud were masked using the QA60 bitmask band, and the remaining pixels were reserved as good-quality observations. Fig. 1A and B presented the spatial distribution of good-quality observation for all pixels and their number from 2015 to 2021, respectively. Over 90% of the pixels have more than 150 good-quality observations from 2015 to 2021. Since the Sentinel-2 was launched in June 2015, the data available in 2015 were insufficient to cover the entire coastal zone of China. Thus, we combined the pixels from 2015 and 2016 to comprise the good-quality observations for 2016. Several studies indicate that atmospheric correction is not necessary for applications not involving complex spectral analysis (Lin et al., 2015; Song et al., 2001); hence, no extra atmospheric correction was applied to the Level-1C Sentinel-2 data in this study. Leveraging the temporal aggregation function of GEE, all available good-quality pixels over a year were composited into a single image by calculating the median of all values at each pixel across the stack of all bands, resulting in high-quality composite images for each year from 2016 to 2021. Compared with the original images, using the median image significantly reduced the size of the dataset, and thus resulting in a higher quality composite image which make the analysis much easier and faster (Tassi and Vizzari, 2020). With the above method, the monthly time series images from 2016 to 2020 were then created by generating high-quality composite images for each month.

Four spectral indices were extracted from Sentinel-2 images to enhance the information on coastal aquaculture ponds and their surrounding dams: the normalized difference vegetation index (NDVI) (Tucker, 1979), the normalized difference water index (NDWI) (McFeeters, 1996), the modified normalized difference water index (mNDWI) (Xu, 2006), and the normalized difference built-up index (NDBI) (Zha et al., 2003). NDWI and mNDWI can greatly strengthen the information of coastal aquaculture ponds, whereas NDVI and NDBI can help enhance the features of the dams surrounding them, which are typically covered with vegetation, gravel, or an impervious surface. These indices are defined as Eqs. (1), (2), (3) and (4):

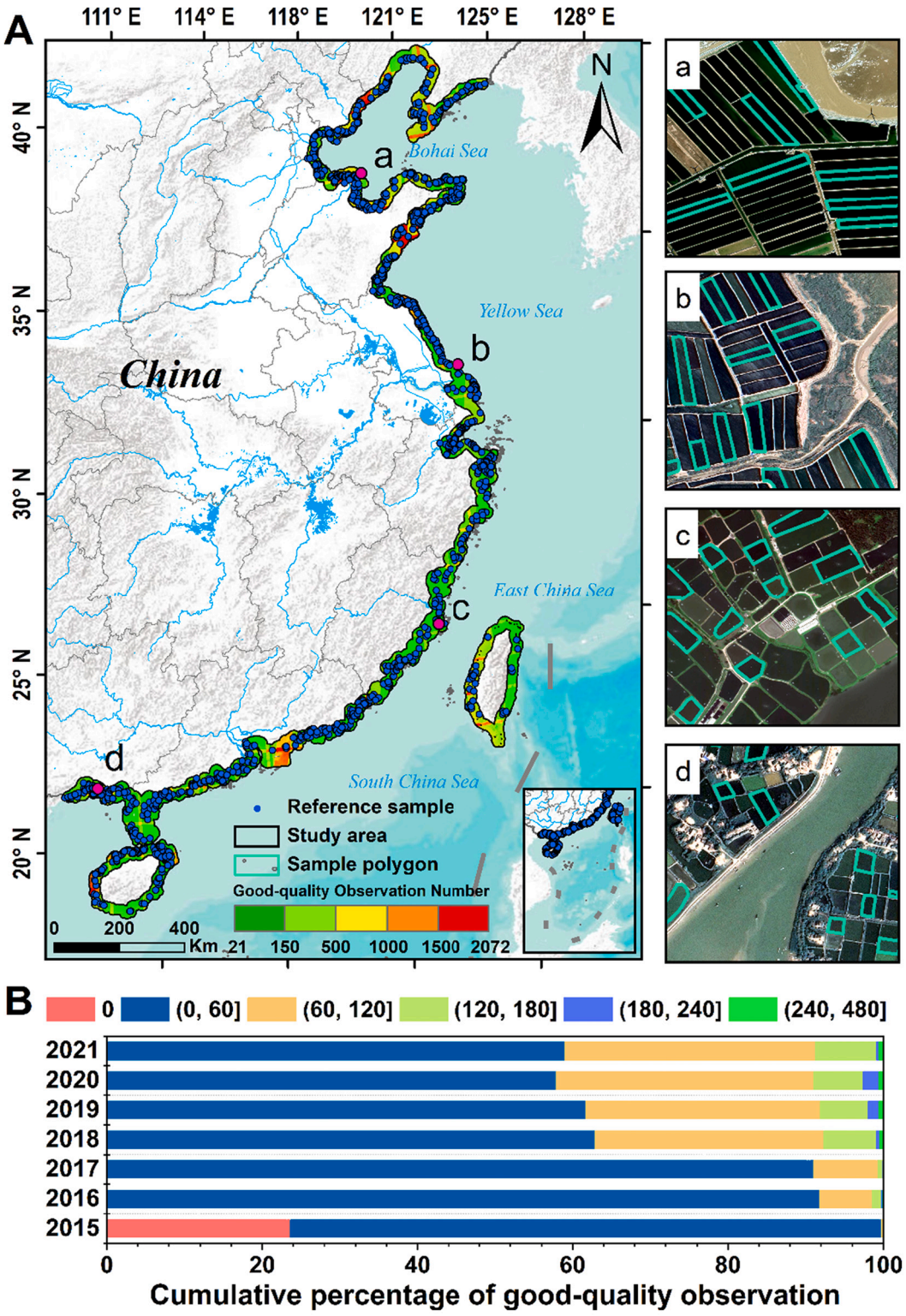

Fig. 1. General information of the study area: (A) presents the geographic location of the study area, the sample distributions of various wetland types, and the spatial distributions of Sentinel-2 good-quality observation number, and (a-d) presents typical examples of coastal aquaculture ponds manually delineated from Google Earth images in 2021, and (B) shows the available Sentinel-2 image numbers for the study area from 2015 to 2021.

$$\mathrm{NDVI} = \frac{\rho_{nir} - \rho_{red}}{\rho_{nir} + \rho_{red}} \quad (1)$$

$$\mathrm{NDWI} = \frac{\rho_{green} - \rho_{nir}}{\rho_{green} + \rho_{nir}} \quad (2)$$

$$\mathrm{mNDWI} = \frac{\rho_{green} - \rho_{swir}}{\rho_{green} + \rho_{swir}} \quad (3)$$

$$\mathrm{NDBI} = \frac{\rho_{swir} - \rho_{nir}}{\rho_{swir} + \rho_{nir}} \quad (4)$$

where ρ_{green}, ρ_{red}, ρ_{nir}, and ρ_{swir} are green (560 nm), red (665 nm), near-infrared (842 nm), and short-wave infrared (1610 nm) bands of Sentinel-2 images.

2.2.2. Reference sample database

In this study, surface water bodies in the coastal area were classified into several categories, including coastal aquaculture pond, salt pan, and other surface water bodies without obvious dams such as lake, river, and lagoon (Table 1). Reference samples of these surface water bodies in 2021 (Fig. 1A) were collected from a series of ground surveys and various collaborations. The acquisition data provided by collaborators varied and applied their own described system for classification. Consequently, using the latest Google Earth images, we validated and modified these sample data to ensure their accuracy, and then relabeled them in a standard format according to the classification system used in our study. For the regions lacking adequate sample data, we used visual interpretation method to obtain sample data based on high-resolution images in Google Earth. Samples were further categorized into coastal aquaculture ponds (AP) and non-coastal aquaculture ponds (Non-AP). Using images from 2015 to 2020, we checked and modified the sample data acquired in 2021 to maintain its validity through visual interpretation and obtained sample data between 2016 and 2021. Finally, we generated 1626 (AP: 817, Non-AP: 809), 1679 (AP: 857, Non-AP: 822), 1758 (AP: 891, Non-AP: 867), 1801 (AP: 912, Non-AP: 889), 1961 (AP: 972, Non-AP: 989) and 2000 (AP: 991, Non-AP: 1009) reference samples for each year from 2016 to 2021, respectively. These samples were used to validate the generated results in this study. Moreover, we manually mapped 500 sample polygons of coastal aquaculture ponds across the entire coast of China using the 2021 sample points and the latest Google Earth images (Fig. 1A) which were ultimately used to determine segmentation scales, generate classification rules, and validate the generated results.

2.2.3. Other datasets

Digital elevation model (DEM), provided by the Shuttle Radar Topography Mission with 30-m spatial resolution, was used in this study to generate topographic information such as elevation and slope. Three global 10-m resolution land cover datasets, including the Dynamic World (https://dynamicworld.app), ESA_Worldcover (https://esa-worldcover.org/en), and FROM-GLC10 (http://data.ess.tsinghua.edu.cn) were used to compare with the result of coastal aquaculture ponds generated by this study. The FROM-GLC10 (Gong et al., 2019) and ESA Worldcover (Zanaga et al., 2021) provide global land cover products utilizing training sample-based machine learning methods in 2017 and 2020, respectively. The Dynamic World (Brown et al., 2022) offers a near real-time global land cover dataset since 2015 using the deep learning method. All of these datasets lack a separate category for coastal aquaculture ponds, instead classifying them as water body with other surface water bodies. However, the regular shapes of coastal aquaculture ponds can still be identified in these products, allowing them to be used for comparison with our results.

Table 1
Water body classification system used in this study.

Category	Description	Image example	Field photo
Coastal aquaculture pond	Surface water body used for aquaculture with regular shape and close to a river or the sea		
Salt pan	Artificial flat depression ground covered with salt and other minerals and close to the sea	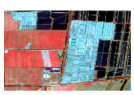	
Other surface water body	Natural or artificial surface water body without artificial dams.		

2.3. Methodologies for delineating coastal aquaculture ponds

In this study, an optimized method was developed to classify coastal aquaculture ponds by combining simple noniterative clustering (SNIC) and hierarchical decision trees (HDT), named as SNIC-HDT. In order to achieve large-scale coastal aquaculture pond mapping, the entire study area was first subdivided into 3° × 3° grids and then subjected to the SNIC-HDT method for each grid. Using this approach, we produced the annual China's national coastal aquaculture pond maps from 2016 to 2021, named China_CAP, following the workflow in Fig. 2. To further explain the workflow, an example (Fig. 2A-F) was provided to demonstrate the classification process of coastal aquaculture ponds.

2.3.1. Generating landscape objects by the SNIC

The SNIC was used to segment homogeneous landscape objects in this study. SNIC is an improved version of the well-known simple linear iterative clustering (SLIC) superpixel segmentation algorithm and has been widely used in object-oriented land cover classification (Achanta and Süsstrunk, 2017; Hemati et al., 2021; Tassi and Vizzari, 2020). In this study, we improved the accuracy of image segmentation by highlighting the outlines of coastal aquaculture ponds using the spectral indices presented in Section 2.2.1. The key parameter of the SNIC algorithm is 'SIZE', which relates to the size of the target object, as well as several optional parameters, such as the compactness factor, connectivity, and neighborhood size (Tassi and Vizzari, 2020; Mahdianpari et al., 2020).

A fixed single empirical segmentation threshold is insufficient to effectively extract aquaculture ponds with different sizes and shapes across all coastal zones in China. Therefore, to obtain reasonable segmentation scales, we utilized optimal scale analysis for coastal aquaculture ponds in China. First, under extensive field surveys and the visual interpretation based on the latest Google Earth imagery, the entire coastal zones of China were divided roughly into three sections, as shown in regions A-C in Fig. 3, according to sizes, shapes, and farming methods of aquaculture ponds. Fig. 3 also depict the most typical coastal aquaculture ponds with distinct size and shape features in three regions, respectively. Region A mainly includes coastal areas of Liaoning, Hebei, Shandong, and Tianjin provinces where coastal aquaculture ponds are distributed in low-lying areas with large sizes and rectangular shapes. In Region B which includes Jiangsu and Shanghai provinces' coastal areas where coastal aquaculture ponds are mostly on coastal plains and are typically smaller than those in Region A. Region C encompasses the remaining coastal provinces of China, where coastal aquaculture ponds are densely distributed across the estuaries, bays, and deltas and have small sizes and approximately square shapes. Second, we selected 200 typical coastal aquaculture ponds in each region and extracted the NDWI standard deviation (SD) curves of their segmentation results at different scales from 5 to 30 (Fig. 4). Then, we obtained the reference value of NDWI SD being 0.12 for coastal aquaculture ponds by extracting NDWI SD values of the sample polygons described in Section 2.2.2. Finally, as shown in Fig. 4, we determined the optimal segmentation scales for each region by combining the reference NDWI SD of coastal aquaculture ponds with the curves obtained in the second step. As a result, the segmentation scales for Regions A, B, and C were determined to be 23, 17, and 13, respectively.

2.3.2. Extracting coastal aquaculture pond objects by hierarchical decision trees

In coastal zones, various surface water bodies may be misclassified as aquaculture ponds, such as salt pans, reservoirs, and lagoons. They have spectral characteristics similar to those of coastal aquaculture ponds. Moreover, salt pans have regular-shaped dams and similar sizes, making them easily confused with coastal aquaculture ponds (Fig. 7). The coastal zone's flooded paddy fields may also have a negative impact on

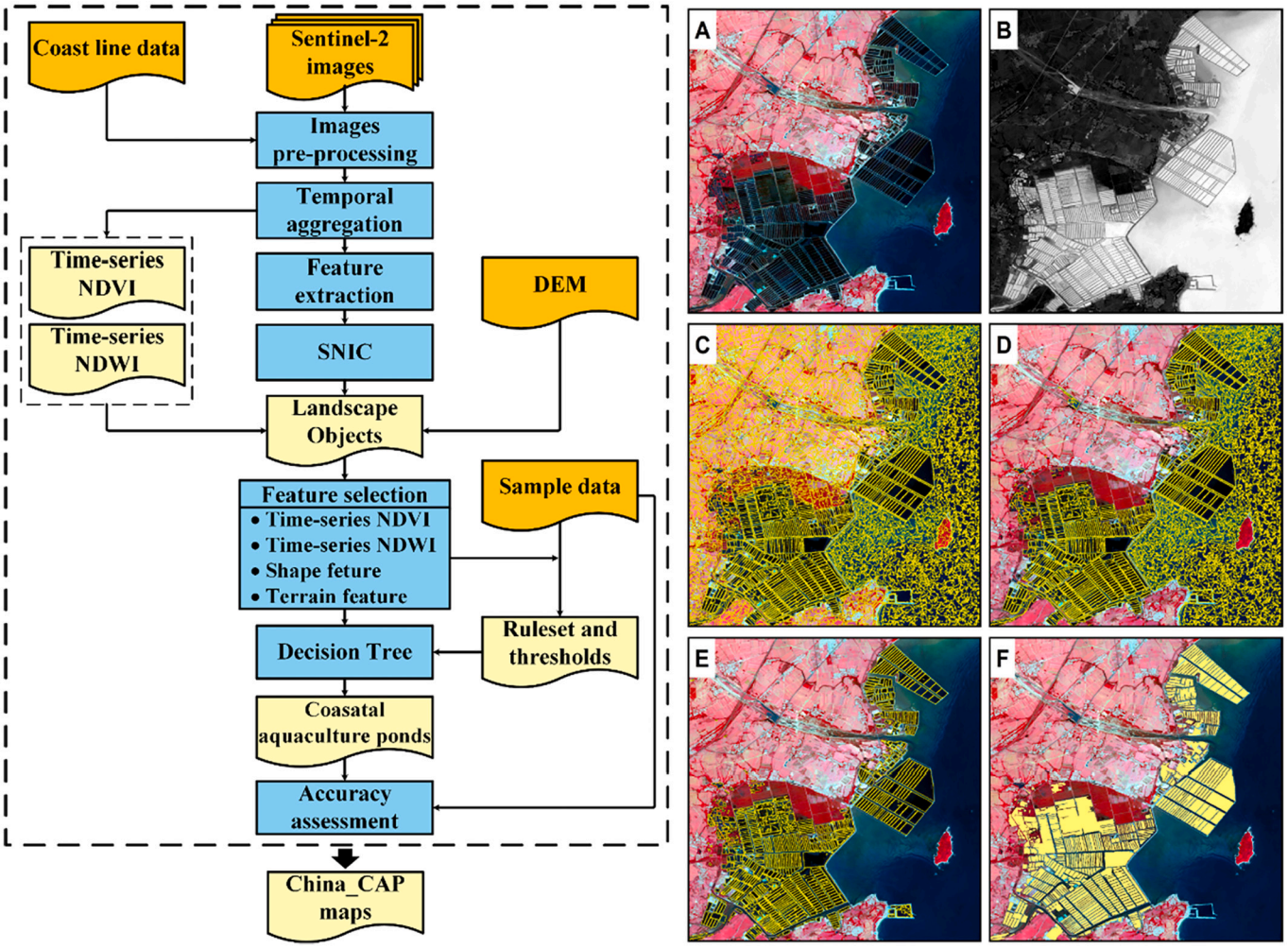

Fig. 2. General workflow of SNIC-HDT. Sub-figs. A-F present the example results of each step of SNIC-HDT in this study: (A) Image preprocessing, (B) Image feature extraction, (C) Image segmentation by SNIC, (D-E) Process of decision tree classification, and (F) Final coastal aquaculture pond product.

the accurate extraction of coastal aquaculture ponds. Due to these similarities, the identification of coastal aquaculture ponds is fraught with uncertainty. As illustrated in Fig. 5, in this study, spectral indices, shapes, terrain conditions, and temporal characteristics were jointly used in designing hierarchical classification trees to extract coastal aquaculture ponds. Details of the decision tree are described as follows:

First, all landscape objects generated by the above processing were divided into water and non-water objects using NDWI and Otsu's method (OTSU) (Otsu, 1979). OTSU is a common and efficient algorithm and has been widely used in land cover classification (Xu et al., 2011). Particularly, at certain times of the year, as shown in Fig. 6, paddy fields are easily confused with water bodies, resulting in misclassification. Thus, we further excluded potential paddy field objects by examining the NDVI time series for all water objects. Water objects were screened out using Eq. (5).

$$Mean\left(NDWI_{object}\right)\langle OTSU\left(NDWI_{study_{area}}\right)$$

and

$$SD\left(TS\_NDVI_{object}\right)\rangle T1 \tag{5}$$

where $NDWI_{object}$ is the NDWI of each landscape object, and *Mean* ($NDWI_{object}$) is the mean value of $NDWI_{object}$. $NDWI_{study\_area}$ is NDWI of the total study area, and *OTSU* ($NDWI_{study\_area}$) is the value of $NDWI_{study\_area}$ using the Otsu algorithm. TS_NDVI_{object} represents the time series *NDVI* values for each object in a year, and *SD* (TS_NDVI_{object}) is the SD value of TS_NDVI_{object}. $T1$ is the threshold of *SD*. To obtain a reasonable threshold, we calculated the SD value of the NDVI time series for all sample polygons of the coastal aquaculture ponds and then determined $T1$ as the average of those values. As a result, $T1$ was set to 0.05 for this study.

Second, the salt pan and other temporary water objects were identified from all waterbody objects generated by the previous step. As shown in Fig. 6, unlike coastal aquaculture ponds, salt pans exhibit distinctive seasonal characteristics which tend to change periodically with the season. Due to different climatic and hydrological conditions, however, the seasonal changes in salt pans and other temporary water bodies vary significantly among regions, making it difficult to adopt a fixed pattern to reflect their respective changes. Thus, SD values were employed in this study to measure NDWI variation in different water bodies and to further remove salt pans and other temporary water objects. The rule is as follows.

$$SD\left(TS\_NDWI_{object}\right)\rangle T2 \tag{6}$$

where TS_NDWI_{object} represents the time series *NDWI* values for a water object in a year, and $SD(TS\_NDWI_{object})$ is the *SD* value of TS_NDWI_{object}. Similar to $T1$, $T2$ was determined by calculating SD values of the NDWI time series for all sample polygons from coastal aquaculture ponds. As a result, $T2$ was set to 0.15 for this study.

Third, the objects of coastal aquaculture ponds were further extrac-

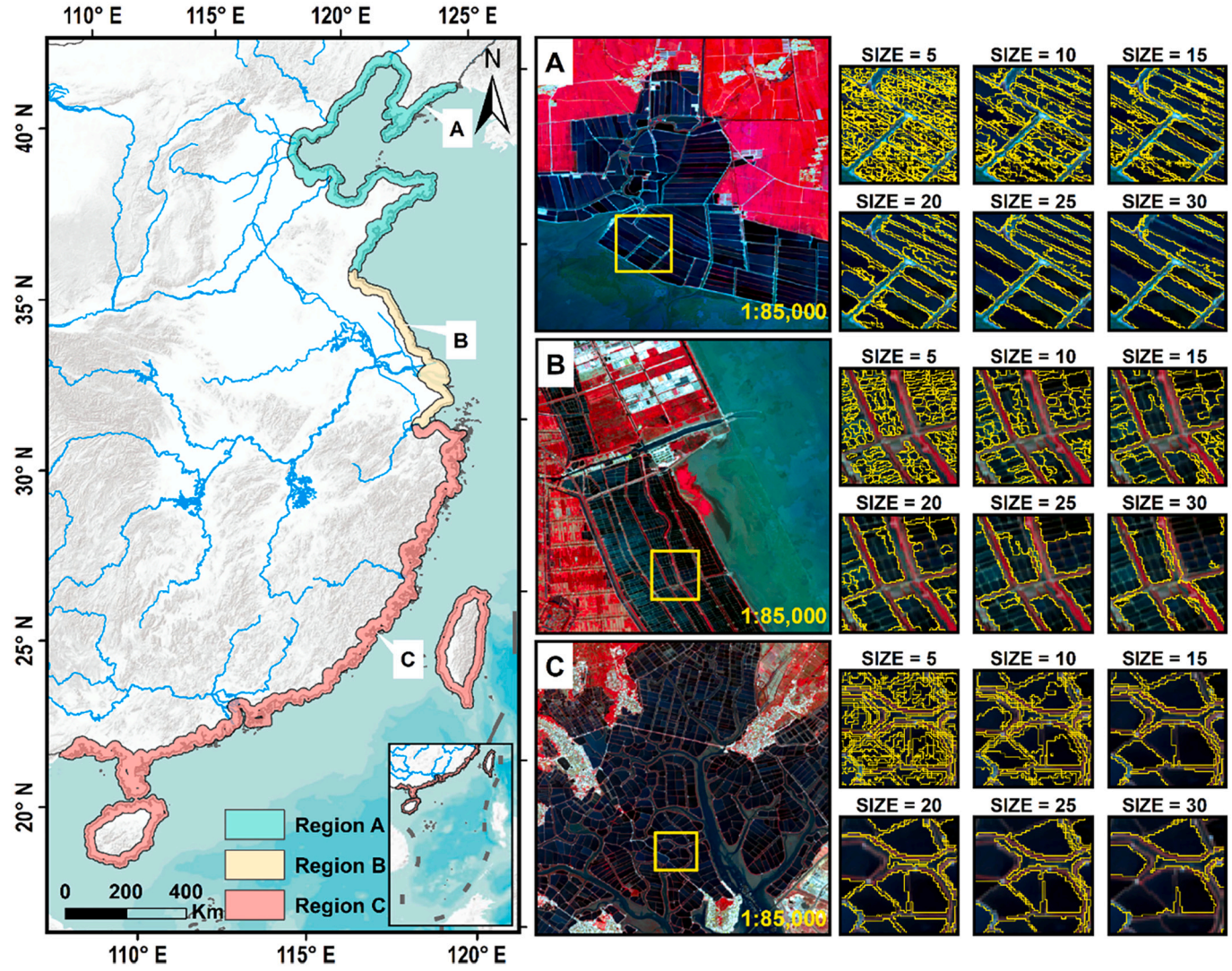

Fig. 3. Locations of typical regions for coastal aquaculture ponds in China. (A), (B), and (C) show the segmentation results of coastal aquaculture ponds in different regions using different segmentation values, respectively.

ted from the classification results in previous steps. Coastal aquaculture ponds are usually located in low-lying coastal areas and have regular-shaped dams. These distinct topographic and shape features can be used to effectively distinguish them from other permanent water bodies. We analyzed topography and shape characteristics of all waterbody objects, including elevation, slope, area, compactness, landscape shape index (LSI), and rectangularity (Table 2), to generate the classification ruleset. As shown in Fig. 7, coastal aquaculture ponds are the most distinguishable from other water bodies by slope and compactness among all features. Accordingly, we used these two indicators to differentiate coastal aquaculture ponds. The results were screened out using Eq. (7).

$$Mean\left(Slope_{object}\right)\langle T3 \; and \; Mean\left(Compactness_{object}\right)\rangle T4 \tag{7}$$

where $Slope_{object}$ and $Compactness_{object}$ denotes the mean value of slope and compactness for each water object, respectively. $T3$ and $T4$ are the thresholds for the slope and compactness values, respectively. They were determined by calculating slope and compactness of all the coastal aquaculture pond sample polygons. Given the varied shape and size of coastal aquaculture ponds, we calculated the corresponding thresholds for Regions A-C as described in Section 2.3.1. Accordingly, $T3$ for Regions A, B, and C was determined to be 1.0, 2.1, and 1.8, while $T4$ was determined to be 1.5, 1.0, and 0.8, respectively.

Finally, the reservoir objects were eliminated from the coastal aquaculture pond results. Reservoirs may exist in the coastal aquaculture pond results generated by the above process as they have similar size, shape, and long-term features. The fundamental distinction between reservoirs and coastal aquaculture ponds is their geographical distribution; reservoirs are frequently isolated, whereas coastal aquaculture ponds have an agglomeration distribution. Thus, a strategy based on determining the spatial relationship among objects was designed in this study to identify the isolated reservoirs. For each object, we first extended its boundary outwards by 50-m and then determined its spatial relationship with the surrounding objects. It was determined to be a reservoir if no surrounding objects intersected with it. Eventually, reservoirs were further identified and eliminated from the results, and accurate coastal aquaculture pond objects were obtained.

2.4. Accuracy assessment

Accuracy assessment was performed using all of the samples between 2016 and 2021 described in Section 2.2. We generated a confusion matrix and four evaluation metrics, namely, overall accuracy, F1 score, user accuracy, and producer accuracy, to evaluate the generated results. Moreover, we also compared our mapping results with the sample

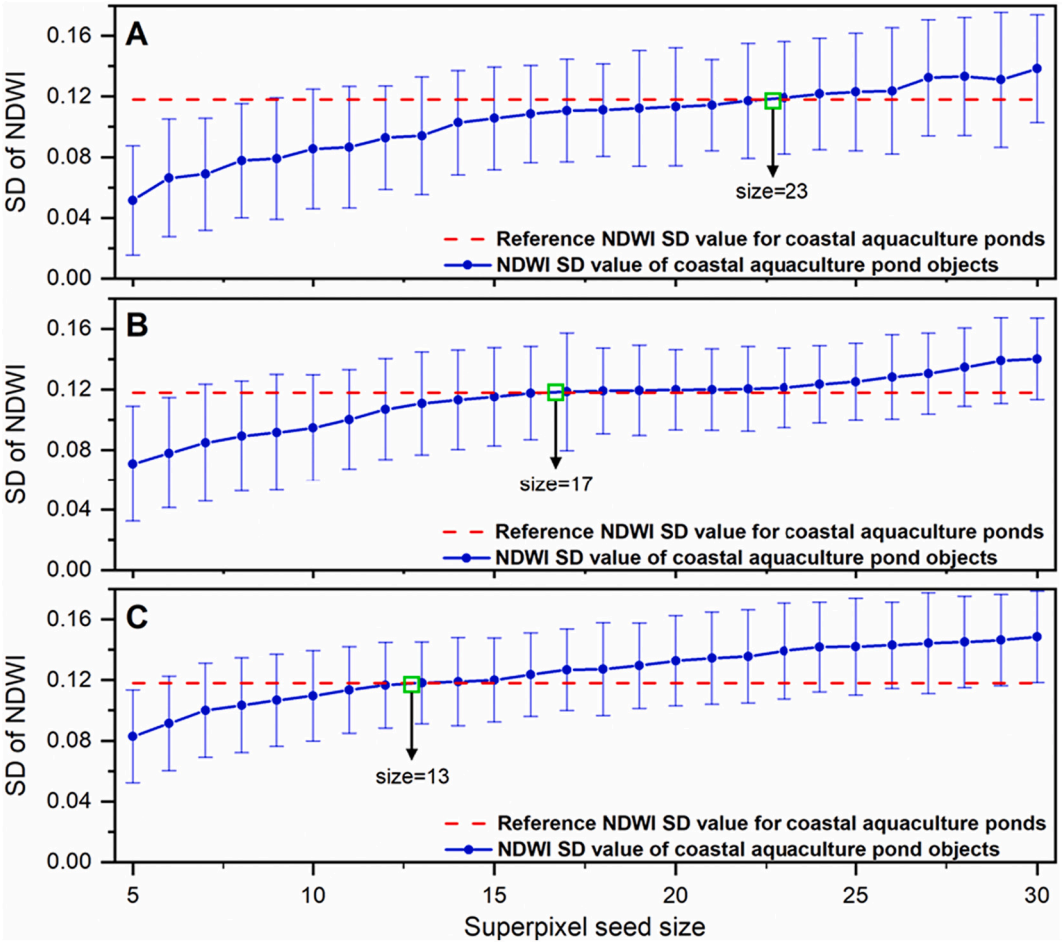

Fig. 4. NDWI SD curves for coastal aquaculture pond objects at different segmentation scales. A, B, and C presents the NDWI SD curves for Region A, Region B, and Region C, respectively.

polygons (Section 2.2) based on a very high resolution Google image (0.54 m) for purposes of evaluating the accuracy of the outlines and shapes of coastal aquaculture ponds derived from our maps.

3. Results

3.1. Accuracy assessment of annual coastal aquaculture pond maps

Table 3 presents the confusion matrix of generated results from 2016 to 2021, demonstrating that our classification results derived by the SNIC-HDT are highly consistent with ground validation samples. The overall accuracy of the classification for each year from 2016 to 2021 was higher than 90%, and the F1 scores for the coastal aquaculture pond category were larger than 0.90. Both producer's accuracy (PA) and user's accuracy (UA) of coastal aquaculture ponds were larger than 89%.

To further evaluate the accuracy of detailed shapes and outlines from the SNIC-HDT, we compared the coastal aquaculture ponds generated in this study with sample polygons based on Google Earth images at 0.54 m spatial resolution. As shown in Fig. 8, the outlines and shapes of coastal aquaculture ponds in China_CAP matched well with the high-precision results obtained through manual digitization. Our results showed a strong correlation with the manually digitized results in area, LSI, and compactness, indicating that our maps provide reliable consistency in terms of on-ground reality.

3.2. Spatial extent of China's coastal aquaculture ponds in 2021

Fig. 9 illustrates the spatial distribution of coastal aquaculture ponds and their national and provincial areal extents in 2021. Coastal aquaculture ponds were widely observed along China's coasts, covering a total area of 8628.79 km^2. As specifically shown in Fig. 9A, coastal aquaculture ponds were densely concentrated in the following five regions (Fig. 9A(1)–(5)): the Bohai Bay, coastal plains of Jiangsu Province, Dongshan Bay and Zhao'an Bay of Fujian Province, Zhelin Bay of Guangdong Province, and Pearl River Delta. Coastal aquaculture ponds in these areas accounted for more than 70% of the total in China. As shown in Fig. 9B and C, Shandong had the largest coastal aquaculture pond area (2133.68 km^2, 24.73%), followed by Guangdong (1662.68 km^2, 19.27%), Hebei (948.31 km^2, 10.99%), and Liaoning (922.15 km^2, 10.69%). In total, these four provinces accounted for 65.68% of China's total coastal aquaculture pond area.

3.3. Interannual changes of coastal aquaculture pond areas from 2016 to 2021

Fig. 10 depicts the spatially varied changes of coastal aquaculture ponds. From 2016 to 2021, the total area of coastal aquaculture ponds in China experienced a consistent decline (Fig. 10C), from 9768.76 km^2 in 2016 to 8628.79 km^2 in 2021, with a net loss of 1139.97 km^2 and 13.21%. Specifically, the inter-annual area change of coastal aquaculture ponds can be divided into two phases: a significant reduction from 2016 to 2018 (a loss of 636.92 km^2) and a moderate reduction from 2019 to 2021 (a loss of 306.94 km^2).

There was evident heterogeneity in the changes of aquaculture ponds during 2016–2021 among provinces (Fig. 10A-B). The most remarkable areal reduction of coastal aquaculture ponds occurred in Zhejiang, with

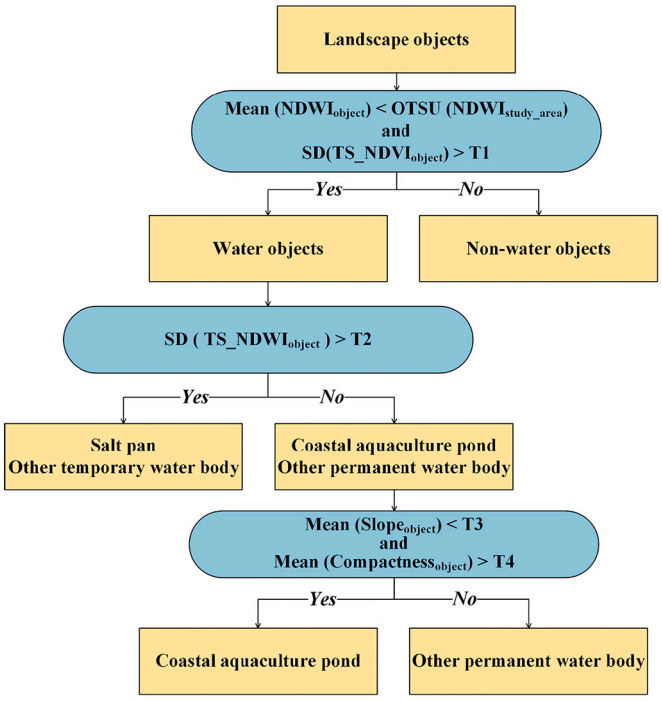

Fig. 5. An example of the hierarchical decision tree used for mapping coastal aquaculture ponds. NDWI$_{object}$, TS_NDWI$_{object}$, Slope$_{object}$, and Compactness$_{object}$ denote the NDWI value, time series NDWI value, slope, and compactness for each image object, respectively. T1 ~ T4 are the thresholds to distinguish coastal aquaculture pond objects.

a rate of 38.24% and an average loss rate of approximately 24.63 km^2 per year, followed by Guangdong (27.93% and 77.49 km^2) and Jiangsu (19.87% and 28.09 km^2). In contrast, coastal aquaculture ponds in Fujian and Tianjin experienced areal increases, with increase rate of 7.24% and 2.13%, respectively. Four typical regions where distinct changes occurred in coastal culture ponds between 2016 and 2021 were presented in Fig. 10a-d. Changes in coastal aquaculture ponds during these years could be clearly observed on China_CAP maps.

4. Discussion

4.1. Effectiveness and robustness of the SNIC-HDT

Based on time series Sentinel-2 images and the GEE platform, we developed an effective approach (SNIC-HDT) for mapping national-scale coastal aquaculture ponds by combining SNIC object segmentation and HDT. The SNIC-HDT performed well in classifying coastal aquaculture ponds and thus achieved the first consistent national coastal aquaculture pond dataset in China with a 10-m spatial resolution (China_CAP). Specifically, the improvements of the SNIC-HDT over previous methods are primarily based on two points.

First, instead of mapping coastal aquaculture ponds across the country using a fixed segmentation scale and classification rule, this study fully considers the spatial heterogeneity of coastal aquaculture ponds and performs accurate segmentation and classification with different sizes and shapes. Due to the markedly diverse morphologies of coastal aquaculture ponds (Fig. 3) affected by variable geographic, climatic conditions, and aquaculture types, we first divided the entire

Table 2
Description and formulas of the three shape metrics used in this study.

Metric	Description	Formula
LSI	Describing the curvature of the object's shape	$\frac{0.25*Perimeter}{\sqrt{Area}}$
Compactness	Describing the curvature and compactness of the object's shape	$\sqrt{\frac{Area}{Bi}}, Bi = \frac{Perimeter^2}{4\pi}$
Rectangularity	Reflecting the degree to which an object fills its external rectangle	$\frac{Area}{Area_{mbr}}$

Note: $Area_{mbr}$ is the area of the object's minimum bounding rectangle.

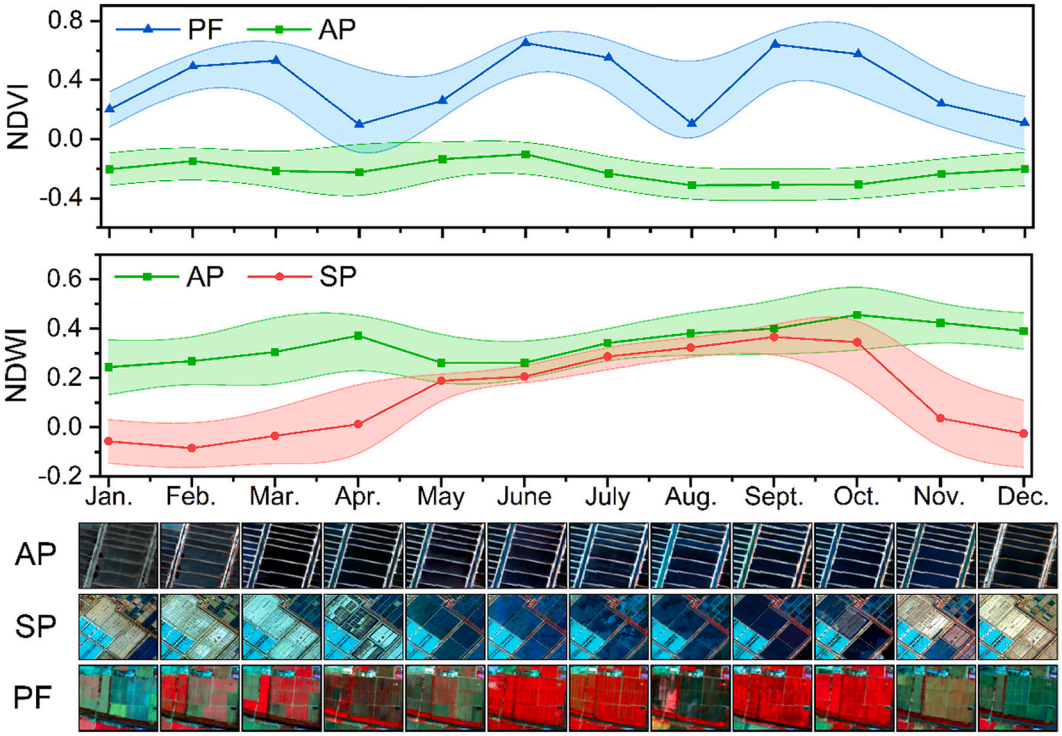

Fig. 6. NDWI, NDVI and landscape change in coastal aquaculture ponds (AP), salt pans (SP), and paddy fields (PF) for each month in a year.

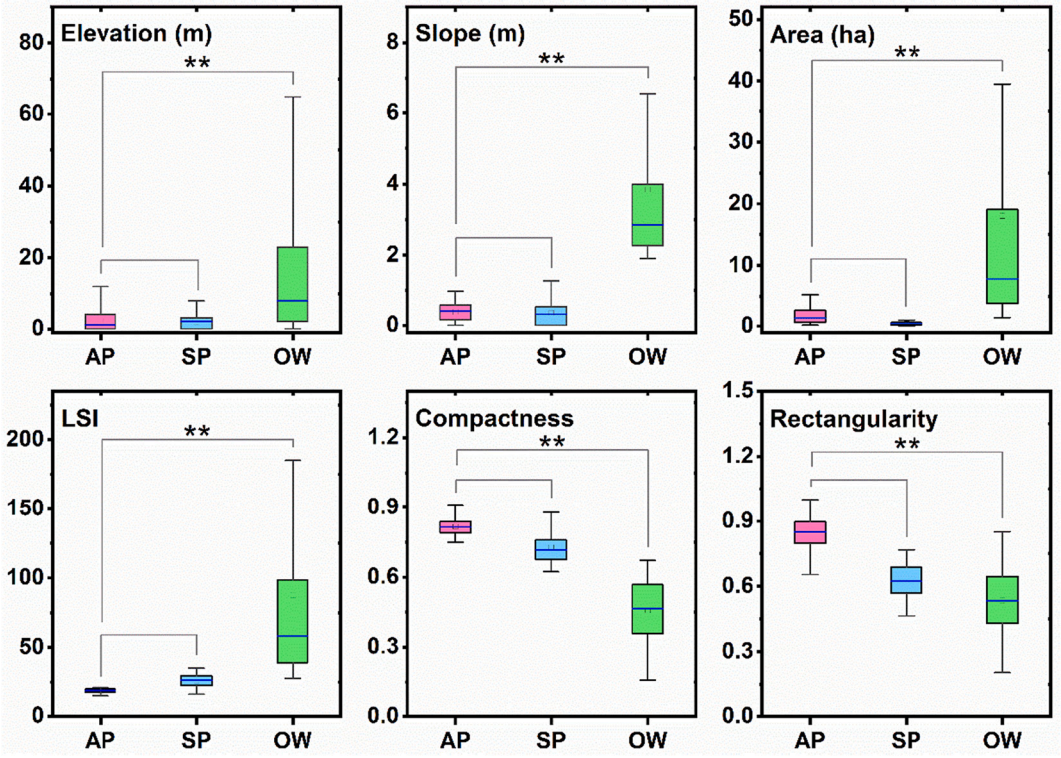

Fig. 7. Comparative boxplots of six metrics, namely, elevation, slope, area, LSI, compactness, and rectangularity, among coastal aquaculture pond (AP), salt pan (SP), and other water body (OW) objects. Note that the "**" indicates that the difference is significant at the 0.05 level.

Table 3
Confusion matrix of result validation based on samples.

Date	Class	AP	Non-AP	Total	UA (%)	F1 score	OA (%)
2016	AP	738	71	809	91.22	0.90	90.77
	Non-AP	79	738	817	90.33	0.90	
	Total	817	809	1626			
	PA (%)	90.33	91.22				
2017	AP	794	74	868	91.47	0.92	91.84
	Non-AP	63	748	811	92.23	0.92	
	Total	857	822	1679			
	PA (%)	92.65	91.00				
2018	AP	811	92	903	89.81	0.90	90.22
	Non-AP	80	775	855	90.64	0.90	
	Total	891	867	1758	–	–	
	PA (%)	91.02	89.39	–	–	–	
2019	AP	846	90	936	90.38	0.92	91.34
	Non-AP	66	799	865	92.37	0.91	
	Total	912	889	1801			
	PA (%)	92.76	89.88				
2020	AP	889	91	980	90.71	0.91	91.13
	Non-AP	83	898	981	91.54	0.91	
	Total	972	989	1961			
	PA (%)	91.46	90.80				
2021	AP	921	84	1005	91.64	0.92	92.30
	Non-AP	70	925	995	92.96	0.92	
	Total	991	1009	2000			
	PA (%)	92.94	91.67				

Note: AP means coastal aquaculture pond, while Non-AP means other water body. UA means user's accuracy, PA means producer's accuracy, and OA means overall accuracy.

study area into three typical regions based on size, shape, and farming mode of coastal aquaculture ponds. Then, by determining the optimal segmentation scale for each region, we accurately segmented coastal aquaculture ponds with different morphologies. The reasonable rules of the decision trees for each region were determined by assessing topographic and shape characteristics. Applying heterogeneous classification rules for different regions can further guarantee the classification accuracy of coastal aquaculture ponds.

Second, in addition to the commonly used features extracted from a single image, such as spectral and topographic features, the SNIC-HDT incorporated time series features into establishing HDT and thus effectively distinguished coastal aquaculture ponds from other easily confused water bodies. Based on monthly time series Sentinel-2 images, we extracted time series NDWI values for each waterbody object throughout a year and further obtained their changing seasonal patterns. A decision tree model based on such changing features was then developed to separate coastal aquaculture ponds correctly from other waterbodies with similar spectra, size, form, and texture.

The SNIC-HDT incorporates optimal segmentation scale analysis and temporal features to accurately identify coastal aquaculture ponds with different sizes and shapes. The required thresholds can be automatically obtained through statistical analysis of sample data which is highly flexible and reliable. Accordingly, the SNIC-HDT can be easily adapted to other coastal zones worldwide, providing finer data on coastal aquaculture ponds and strongly supporting the study of coastal ecological issues such as mangrove deterioration and offshore nutrient pollution.

4.2. *Fine observations of national coastal aquaculture pond datasets*

Compared to the existing 30-m products of coastal aquaculture pond in China, China_CAP provide the latest annual satellite observation results (2016–2021) with a finer spatial resolution (10-m). Moreover, China_CAP presents more precise results by employing dense time series images to track seasonal variations, and thus effectively distinguishes coastal aquaculture ponds from other water bodies. We also compared China_CAP to three 10-m resolution land cover datasets: Dynamic World, ESA_Worldcover, and FROM-GLC10 (Section 2.2.3). Due to the varying dates of the above three products, to ensure comparability, we selected the regions with the slighter change between 2016 and 2021

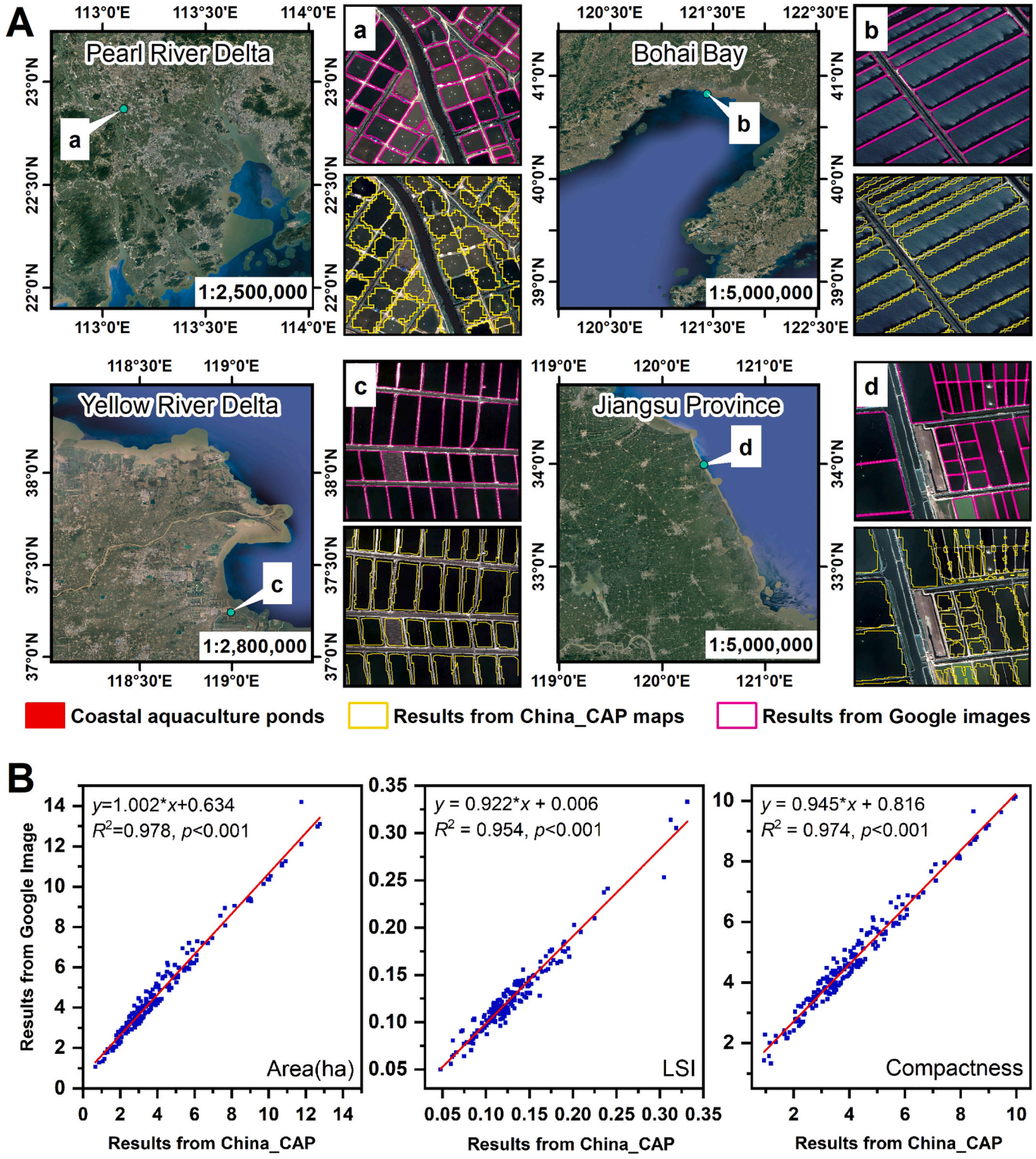

Fig. 8. The comparison between the SNIC-HDT results and the corresponding results manually delineated from Google Earth images. (A) compares the two results visually, whereas (B) analyzes their correlation in terms of area, LSI, and compactness.

based on China_CAP for comparison (Fig. 11). China CAP provides a more accurate extent of coastal aquaculture ponds, and this difference in extent could be attributed to different classification approaches. All the three land cover datasets were produced by pixel-based supervised classification method, which relies on vast training samples and are easily affected by landscape complexity, invariably resulting in the "salt and pepper" effect. Narrow dams and drainage channels around aquaculture ponds were also difficult to be identified using this training sample-based method accurately. In contrast, China_CAP was generated from a novel object-oriented approach integrating superpixel segmentation and knowledge-based classification, thereby avoiding the "salt and pepper" effect and enabling accurate detection of dams in the majority of coastal aquaculture ponds.

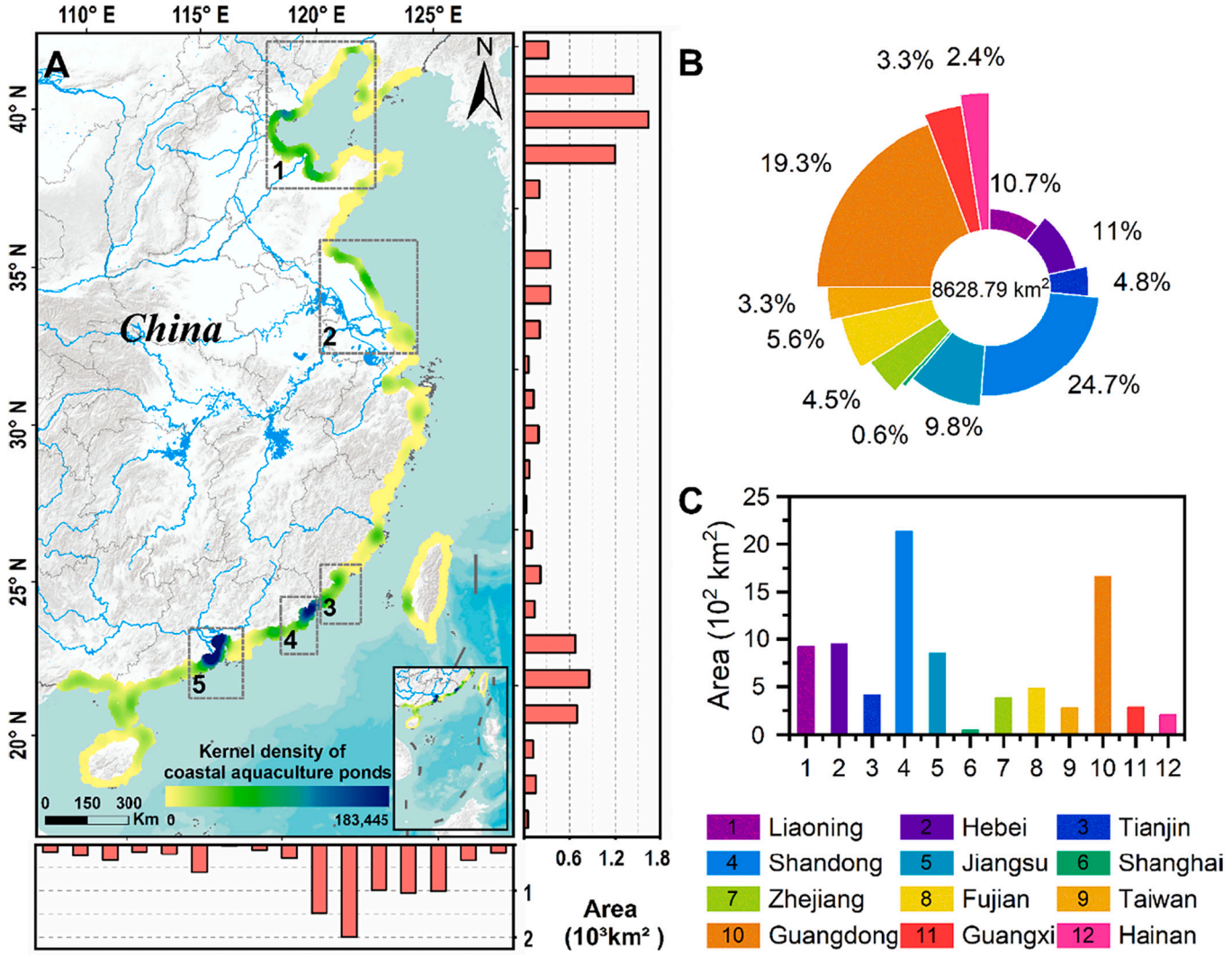

Fig. 9. Distribution and areal statistics of coastal aquaculture ponds in China in 2021. (A): The kernel density map of coastal aquaculture ponds in China in 2021; (1)–(5) present the most densely distributed areas of coastal aquaculture ponds from north to south. (B): The area proportion of coastal aquaculture ponds in each province. (C): The provincial areal statistics of coastal aquaculture ponds. Coastal aquaculture ponds in Guangdong Province include those of Hong Kong and Macao.

4.3. Management implications of coastal ecosystems following coastal aquaculture pond changes

Various aquatic products from coastal aquaculture ponds can contribute to global food security needs and bring substantial economic benefits to coastal areas (Tacon, 2020). As an essential part of coastal ecosystems, aquaculture ponds could be used to control the invasion of *Spartina alterniflora* and provide alternative habitats for migratory birds (Li et al., 2022; Ottinger et al., 2016). On the other hand, the extensive expansion of coastal aquaculture ponds encroaches upon natural wetlands such as tidal flats, mangroves, and salt marshes (Mao et al., 2021), triggering a series of environmental issues. Thus, sustainable strategies are urgently needed to balance the development of coastal aquaculture ponds and the protection of natural wetland ecosystems in coastal areas. China_CAP can provide up-to-date information on coastal aquaculture pond distributions and high-resolution changes at a 10-m spatial resolution across the coastline of China during 2016–2021, which is vital for formulating and implementing sustainable strategies related to the wise use of coastal wetlands. For example, our results reveal that coastal aquaculture ponds in China have experienced consistent areal decline since the SDG base year (2015) due to the implementation of many national ecological policies, such as "returning ponds to natural wetlands", particularly in some important coastal wetland regions (Fig. 10A). However, two provinces, Fujian and Tianjin, are still expanding their coastal aquaculture in an efficient farming style, experiencing slight areal increases during the five years. The results generated in this study revealed China's transition from sprawl extension to the sustainable development of coastal aquaculture ponds in the face of continued coastal ecosystem degradation. It is of great inspiration for some developing countries whose coastal aquaculture industries are rapidly developing such as countries in South and Southeast Asia, helping them formulate sustainable strategies. Additionally, China_CAP could provide data in support of the conservation of migratory water birds along the East Asia-Australia Flyway (EAAF) and is of great scientific and practical importance to support the evaluation of SDG 14.2 (sustainably manage and protect marine and coastal ecosystems) and provide a reference for assessing the targets of SDGs 6.6 (protect and restore water-related ecosystems), 13.1 (strengthen resilience and adaptive capacity to climate-related hazards and natural disasters), 15.5 (reduce the degradation of natural habitats, halt the loss of biodiversity), and so on.

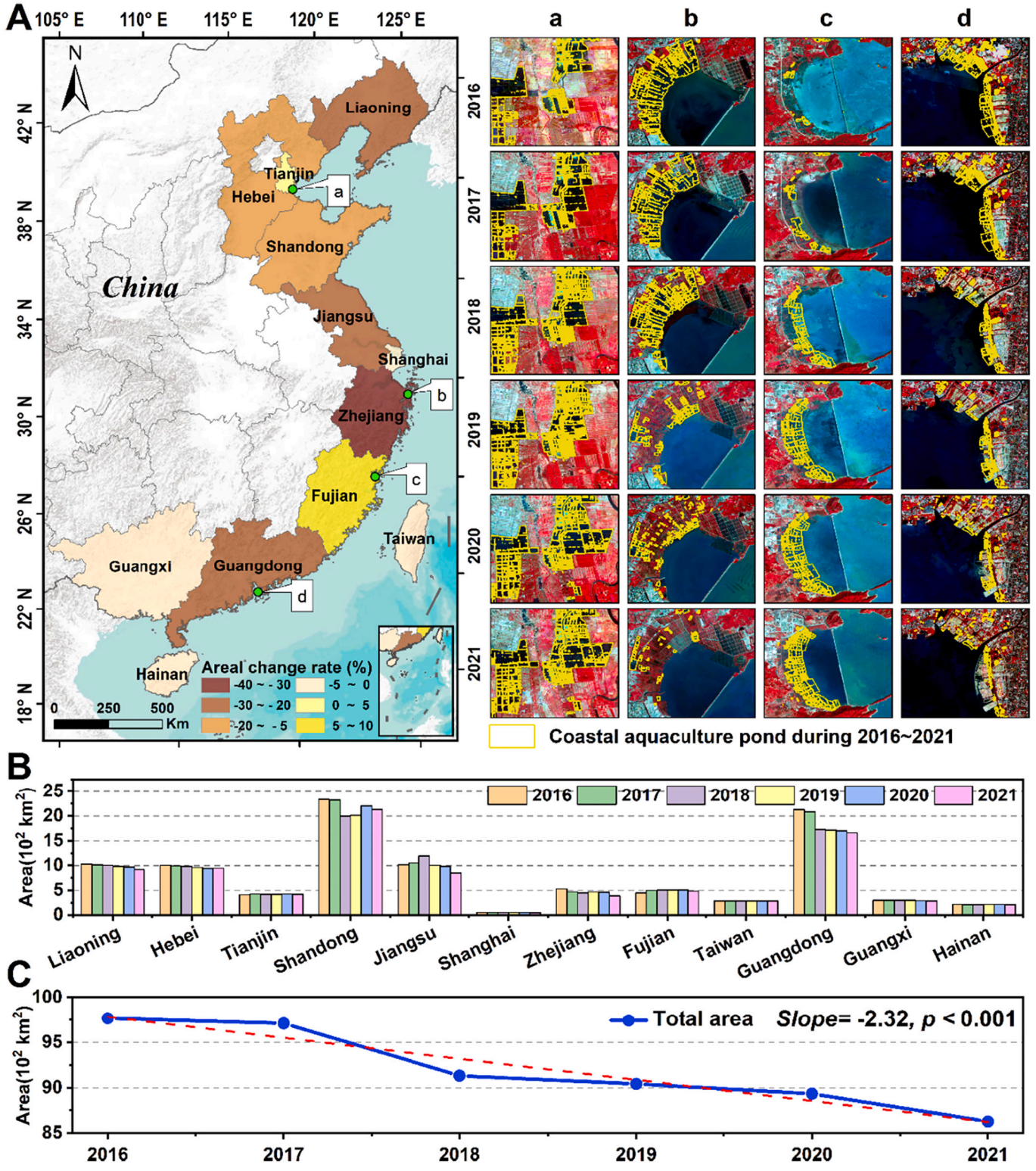

Fig. 10. Spatial distributions and areal changes of coastal aquaculture ponds in China during 2016– 2021. (A) depicts the spatial distributions of areal changes in coastal aquaculture ponds at the provincial scale from 2016 to 2021, and (a-d) present four important wetland areas where distinct changes occurred in coastal culture ponds, respectively. (B) and (C) show area changes in area of coastal aquaculture pond at the province and national scales from 2016 to 2021.

5. Conclusions

The national coastal aquaculture pond dataset of China with high resolution (10-m and annual) from 2016 to 2021 (China_CAP) is first generated in this study by developing an effective approach (SNIC-HDT) on the Sentinel 2 time-series images. The SNIC-HDT incorporates the optimal segmentation scale analysis and temporal features into the classification of coastal aquaculture ponds and thus effectively identifies them with different sizes and shapes. The China_CAP datasets have an overall classification accuracy higher than 90% and reveal that China's

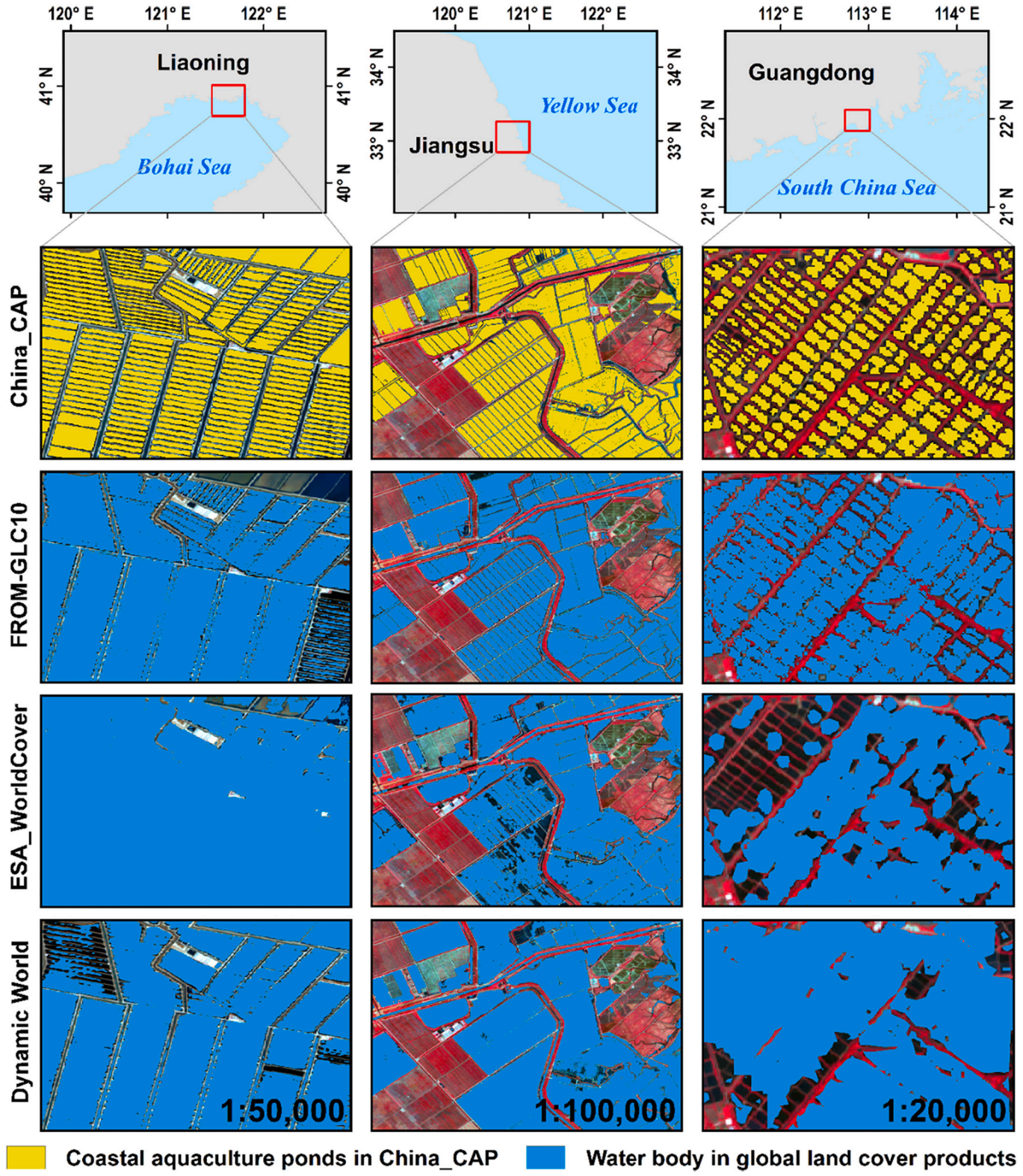

Fig. 11. Comparison of coastal aquaculture ponds between China_CAP and three global 10-m resolution land cover datasets, including the Dynamic World, ESA_Worldcover, and FROM-GLC10.

coastal aquaculture ponds experienced a continuous areal decline since the base year (2015) of SDGs, with a decline rate of 13.21%.The improved method developed in this study could provide a reference for the observation of coastal aquaculture ponds in other countries for global coastal ecosystem sustainability, and the generated dataset at fine resolution can provide a data-supported basis for sustainable planning and management of coastal zones in China and even the world.

CRediT authorship contribution statement

Ming Wang: Methodology, Software, Writing – original draft. **Dehua Mao:** Conceptualization, Validation, Funding acquisition, Writing – review & editing. **Xiangming Xiao:** Writing – review & editing, Validation. **Kaishan Song:** Writing – review & editing, Validation. **Mingming Jia:** Writing – review & editing. **Chunying Ren:** Writing – review & editing. **Zongming Wang:** Writing – review & editing, Validation.

Declaration of Competing Interest

The authors declare that they have no known competing financial interests or personal relationships that could have appeared to influence the work reported in this paper.

Data availability

Data will be made available on request.

Acknowledgments

This research was jointly funded by the National Natural Science Foundation of China (42222103, 42171379, and 42101379), the Science and Technology Development Program of Jilin Province, China (20210101396JC, 20200301014RQ), the Youth Innovation Promotion Association of Chinese Academy of Sciences (2017277, 2021227), the Professional Association of the Alliance of International Science Organizations (ANSO-PA-2020-14), and the Young Scientist Group Project of Northeast Institute of Geography and Agroecology, Chinese Academy of Sciences (2022QNXZ03). Xiangming Xiao was supported by the U.S. National Science Foundation (1911955). We wish to thank the timely help given by Zhiqiang Qiu, Xiaoyu Tan, Jingfa Wang, Yuxin Zhao and Jiarui Chen in processing the large amount of data.

References

Achanta, R., Süsstrunk, S., 2017. Superpixels and polygons using simple non-iterative clustering. In: 2017 IEEE Conference on Computer Vision and Pattern Recognition (CVPR). Presented at the 2017 IEEE Conference on Computer Vision and Pattern Recognition (CVPR), pp. 4895–4904. https://doi.org/10.1109/CVPR.2017.520.

Ahmed, N., Thompson, S., Glaser, M., 2019. Global aquaculture productivity, environmental sustainability, and climate change adaptability. Environ. Manag. 63, 159–172. https://doi.org/10.1007/s00267-018-1117-3.

Ali, I., Cao, S., Naeimi, V., Paulik, C., Wagner, W., 2018. Methods to remove the border noise from Sentinel-1 synthetic aperture radar data: implications and importance for time-series analysis. IEEE J. Sel. Top. Appl. Earth Obs. Remote Sens. 11 (3), 777–786. https://doi.org/10.1109/JSTARS.2017.2787650.

Brown, C.F., Brumby, S.P., Guzder-Williams, B., Birch, T., Hyde, S.B., Mazzariello, J., Czerwinski, W., Pasquarella, V.J., Haertel, R., Ilyushchenko, S., Schwehr, K., Weisse, M., Stolle, F., Hanson, C., Guinan, O., Moore, R., Tait, A.M., 2022. Dynamic World, Near real-time global 10 m land use land cover mapping. Sci Data. 9(1), 251. https://doi.org/10.1038/s41597-022-01307-4.

Diniz, C., Cortinhas, L., Pinheiro, M.L., Sadeck, L., Fernandes Filho, A., Baumann, L.R.F., Adami, M., Souza-Filho, P.W.M., 2021. A Large-Scale Deep-Learning Approach for Multi-Temporal Aqua and Salt-Culture Mapping. Remote Sens. 13(8), 1415. https://doi.org/10.3390/rs13081415.

Duan, Y., Tian, B., Li, X., Liu, D., Sengupta, D., Wang, Y., Peng, Y., 2021. Tracking changes in aquaculture ponds on the China coast using 30 years of landsat images. Int. J. Appl. Earth Obs. Geoinf. 102, 102383 https://doi.org/10.1016/j.jag.2021.102383.

FAO, 2020. The State of World Fisheries and Aquaculture 2020. Sustainability in action, Rome.

Fu, Y., Deng, J., Ye, Z., Gan, M., Wang, K., Wu, J., Yang, W., Xiao, G., 2019. Coastal aquaculture mapping from very high spatial resolution imagery by combining object-based neighbor features. Sustainability 11, 637. https://doi.org/10.3390/su11030637.

Gephart, J.A., Golden, C.D., Asche, F., Belton, B., Brugere, C., Froehlich, H.E., Fry, J.P., Halpern, B.S., Hicks, C.C., Jones, R.C., Klinger, D.H., Little, D.C., McCauley, D.J., Thilsted, S.H., Troell, M., Allison, E.H., 2021. Scenarios for global aquaculture and its role in human nutrition. Rev. Fish. Sci. Aquac. 29, 122–138. https://doi.org/10.1080/23308249.2020.1782342.

Gong, P., Liu, H., Zhang, M., Li, C., Wang, J., Huang, H., Clinton, N., Ji, L., Li, Wenyu, Bai, Y., Chen, B., Xu, B., Zhu, Z., Yuan, C., Ping Suen, H., Guo, J., Xu, N., Li, Weijia, Zhao, Y., Yang, J., Yu, C., Wang, X., Fu, H., Yu, L., Dronova, I., Hui, F., Cheng, X., Shi, X., Xiao, F., Liu, Q., Song, L., 2019. Stable classification with limited sample: transferring a 30-m resolution sample set collected in 2015 to mapping 10-m resolution global land cover in 2017. Sci. Bull. 64, 370–373. https://doi.org/10.1016/j.scib.2019.03.002.

Hemati, M.A., Hasanlou, M., Mahdianpari, M., Mohammadimanesh, F., 2021. Wetland mapping of Northern Provinces of Iran using Sentinel-1 and Sentinel-2 in Google Earth Engine. In: 2021 IEEE International Geoscience and Remote Sensing Symposium IGARSS. Presented at the 2021 IEEE International Geoscience and Remote Sensing Symposium IGARSS, pp. 96–99. https://doi.org/10.1109/IGARSS47720.2021.9554984.

Jia, M., Wang, Z., Mao, D., Ren, C., Wang, C., Wang, Y., 2021. Rapid, robust, and automated mapping of tidal flats in China using time series Sentinel-2 images and Google earth engine. Remote Sens. Environ. 255, 112285 https://doi.org/10.1016/j.rse.2021.112285.

Johnson, B., Xie, Z., 2011. Unsupervised image segmentation evaluation and refinement using a multi-scale approach. ISPRS J. Photogramm. Remote Sens. 66, 473–483. https://doi.org/10.1016/j.isprsjprs.2011.02.006.

Lin, C., Wu, C.-C., Tsogt, K., Ouyang, Y.-C., Chang, C.-I., 2015. Effects of atmospheric correction and pansharpening on LULC classification accuracy using WorldView-2 imagery. Inform. Process. Agric. 2, 25–36. https://doi.org/10.1016/j.inpa.2015.01.003.

Li, H., Mao, D., Wang, Z., Huang, X., Li, L., Jia, M., 2022. Invasion of Spartina alterniflora in the coastal zone of mainland China: control achievements from 2015 to 2020 towards the sustainable development goals. J. Environ. Manag. 323, 116242 https://doi.org/10.1016/j.jenvman.2022.116242.

Loberternos, R.A., Porpetcho, W.P., Graciosa, J.C.A., Violanda, R.R., Diola, A.G., Dy, D. T., Otadoy, R.E.S., 2016. An object-based workflow developed to extract aquaculture ponds from airborne LIDAR data: a test case in Central Visayas, Philippines. In: ISPRS - International Archives of the Photogrammetry, Remote Sensing and Spatial Information Sciences 41B8, pp. 1147–1152. https://doi.org/10.5194/isprs-archives-XLI-B8-1147-2016.

Mahdianpari, M., Salehi, B., Mohammadimanesh, F., Brisco, B., Homayouni, S., Gill, E., DeLancey, E.R., Bourgeau-Chavez, L., 2020. Big data for a big country: the first generation of Canadian wetland inventory map at a spatial resolution of 10-m using Sentinel-1 and Sentinel-2 data on the Google earth engine cloud computing platform. Can. J. Remote. Sens. 46, 15–33. https://doi.org/10.1080/07038992.2019.1711366.

Mao, D., Yang, H., Wang, Z., Song, K., Thompson, J.R., Flower, R.J., 2022. Reverse the hidden loss of China's wetlands. Science 376 (6597), 1061. https://doi.org/10.1126/science.adc8833.

Mao, D., Wang, Z., Du, B., Li, L., Tian, Y., Jia, M., Zeng, Y., Song, K., Jiang, M., Wang, Y., 2020. National wetland mapping in China: a new product resulting from object-based and hierarchical classification of landsat 8 OLI images. ISPRS J. Photogramm. Remote Sens. 164, 11–25. https://doi.org/10.1016/j.isprsjprs.2020.03.020.

Mao, D., Wang, Z., Wang, Y., Choi, C.-Y., Jia, M., Jackson, M.V., Fuller, R.A., 2021. Remote observations in China's Ramsar sites: wetland dynamics, anthropogenic threats, and implications for sustainable development goals. J. Remote Sens. 2021 https://doi.org/10.34133/2021/9849343.

McFeeters, S.K., 1996. The use of the normalized difference water index (NDWI) in the delineation of open water features. Int. J. Remote Sens. 17, 1425–1432. https://doi.org/10.1080/01431169608948714.

Otsu, N., 1979. A threshold selection method from gray-level histograms. IEEE Trans. Syst. Man Cybern. 9, 62–66. https://doi.org/10.1109/TSMC.1979.4310076.

Ottinger, M., Clauss, K., Kuenzer, C., 2016. Aquaculture: relevance, distribution, impacts and spatial assessments – a review. Ocean Coast. Manage. 119, 244–266. https://doi.org/10.1016/j.ocecoaman.2015.10.015.

Prasad, K.A., Ottinger, M., Wei, C., Leinenkugel, P., 2019. Assessment of coastal aquaculture for India from Sentinel-1 SAR time series. Remote Sens. 11, 357. https://doi.org/10.3390/rs11030357.

Ren, C., Wang, Z., Zhang, Y., Zhang, B., Chen, L., Xi, Y., Xiao, X., Doughty, R.B., Liu, M., Jia, M., Mao, D., Song, K., 2019. Rapid expansion of coastal aquaculture ponds in China from landsat observations during 1984–2016. Int. J. Appl. Earth Obs. Geoinf. 82, 101902 https://doi.org/10.1016/j.jag.2019.101902.

Song, C., Woodcock, C.E., Seto, K.C., Lenney, M.P., Macomber, S.A., 2001. Classification and change detection using landsat TM data: when and how to correct atmospheric Effects? Remote Sens. Environ. 75, 230–244. https://doi.org/10.1016/S0034-4257(00)00169-3.

Sridhar, P.N., Surendran, A., Ramana, I.V., 2008. Auto-extraction technique-based digital classification of saltpans and aquaculture plots using satellite data. Int. J. Remote Sens. 29, 313–323. https://doi.org/10.1080/01431160701250374.

Sun, Z., Luo, J., Yang, J., Yu, Q., Zhang, L., Xue, K., Lu, L., 2020. Nation-scale mapping of coastal aquaculture ponds with Sentinel-1 SAR data using Google earth engine. Remote Sens. 12, 3086. https://doi.org/10.3390/rs12183086.

Suweis, S., Carr, J.A., Maritan, A., Rinaldo, A., D'Odorico, P., 2015. Resilience and reactivity of global food security. PNAS 112, 6902–6907. https://doi.org/10.1073/pnas.1507366112.

Tacon, A.G.J., 2020. Trends in global aquaculture and aquafeed production: 2000–2017. Rev. Fish. Sci. Aquac. 28, 43–56. https://doi.org/10.1080/23308249.2019.1649634.

Tassi, A., Vizzari, M., 2020. Object-oriented LULC classification in Google earth engine combining SNIC, GLCM, and machine learning algorithms. Remote Sens. 12, 3776. https://doi.org/10.3390/rs12223776.

Tucker, C.J., 1979. Red and photographic infrared linear combinations for monitoring vegetation. Remote Sens. Environ. 8(2), 127–150. https://doi.org/10.1016/0034-4257(79)90013-0.

Virdis, S.G.P., 2014. An object-based image analysis approach for aquaculture ponds precise mapping and monitoring: a case study of tam giang-cau hai lagoon,Vietnam. Environ. Monit. Assess. 186, 117–133. https://doi.org/10.1007/s10661-013-3360-7.

Wang, X., Xiao, X., Zou, Z., Hou, L., Qin, Y., Dong, J., Doughty, R.B., Chen, B., Zhang, X., Chen, Y., Ma, J., Zhao, B., Li, B., 2020. Mapping coastal wetlands of China using time series landsat images in 2018 and Google earth engine. ISPRS J. Photogramm. Remote Sens. 163, 312–326. https://doi.org/10.1016/j.isprsjprs.2020.03.014.

Xia, Z., Guo, X., Chen, R., 2020. Automatic extraction of aquaculture ponds based on Google Earth Engine. Ocean & Coastal Management. 198, 105348. https://doi.org/10.1016/j.ocecoaman.2020.105348.

Xu, H., 2006. Modification of normalised difference water index (NDWI) to enhance open water features in remotely sensed imagery. Int. J. Remote Sens. 27, 3025–3033. https://doi.org/10.1080/01431160600589179.

Xu, X., Xu, S., Jin, L., Song, E., 2011. Characteristic analysis of Otsu threshold and its applications. Pattern Recogn. Lett. 32, 956–961. https://doi.org/10.1016/j.patrec.2011.01.021.

Zanaga, D., Van De Kerchove, R., De Keersmaecker, W., Souverijns, N., Brockmann, C., Quast, R., Wevers, J., Grosu, A., Paccini, A., Vergnaud, S., Cartus, O., Santoro, M., Fritz, S., Georgieva, I., Lesiv, M., Carter, S., Herold, M., Li, L., Tsendbazar, N.-E., Ramoino, F., Arino, O., 2021. ESA WorldCover 10 m 2020 v100. https://doi.org/10.5281/zenodo.5571936.

Zha, Y., Gao, J., Ni, S., 2003. Use of normalized difference built-up index in automatically mapping urban areas from TM imagery. Int. J. Remote Sens. 24, 583–594. https://doi.org/10.1080/01431160304987.

Zhang, Z., Xu, N., Li, Yangfan, Li, Yi, 2022. Sub-continental-scale mapping of tidal wetland composition for East Asia: a novel algorithm integrating satellite tide-level and phenological features. Remote Sens. Environ. 269, 112799 https://doi.org/10.1016/j.rse.2021.112799.